Check for updates

Geophysical Research Letters

RESEARCH LETTER
10.1029/2024GL110456

Key Points:

- Using satellite height change data we document the discovery of a 52 km^2 subglacial lake under the Manson Icefield, Nunavut, Canada
- The lake filled for around 14 years until early 2021 when the level in the center of the lake dropped by 130 m over 30 days
- The outflow volume was around 4 cubic kilometers and created a wide and shallow subglacial channel that could be tracked for over 15 km

Supporting Information:

Supporting Information may be found in the online version of this article.

Correspondence to:

L. Gray,
laurence.gray@uottawa.ca

Citation:

Gray, L., Lauzon, B., Copland, L., Van Wychen, W., Dow, C., Kochtitzky, W., & Alley, K. E. (2024). Tracking the filling, outburst flood and resulting subglacial water channel from a large Canadian Arctic subglacial lake. *Geophysical Research Letters*, *51*, e2024GL110456. https://doi.org/10.1029/2024GL110456

Received 24 MAY 2024
Accepted 13 SEP 2024

© 2024. The Author(s).
This is an open access article under the terms of the Creative Commons Attribution License, which permits use, distribution and reproduction in any medium, provided the original work is properly cited.

Tracking the Filling, Outburst Flood and Resulting Subglacial Water Channel From a Large Canadian Arctic Subglacial Lake

Laurence Gray[1], Benoît Lauzon[1], Luke Copland[1], Wesley Van Wychen[2], Christine Dow[2], Will Kochtitzky[3], and Karen E. Alley[4]

[1]Department of Geography, Environment and Geomatics, University of Ottawa, Ottawa, ON, Canada, [2]Department of Geography and Environmental Management, University of Waterloo, Waterloo, ON, Canada, [3]School of Marine and Environmental Programs, University of New England, Biddeford, ME, USA, [4]Centre for Earth Observation Science, University of Manitoba, Winnipeg, MB, Canada

Abstract We use digital elevation models (DEMs) and ICESat-2 data to study the filling and outflow from a large subglacial lake under Manson Icefield in the Canadian Arctic. When full, the lake is ∼17 × 3 km with an area of 52 km^2. Early in 2021 the ice surface over the center of the lake sank by >140 m implying a subglacial outburst flood of ∼4 km^3. Rapid outflow occurred over ∼30 days at an average rate of ∼1,500 m^{3}s^{-1} resulting in the formation of a single ∼15 km subglacial outflow path detectable from post-outflow surface depression. The shape of the surface depression, 600–800 m wide by 2–4 m deep, reflects the shape of the subglacial channel prior to closure. Downstream ice movement appears unaffected by the outflow. After outflow ends the surface depression persisted over weeks, apparently dependent on the difference between water and overburden pressures.

Plain Language Summary Using satellite observations, we discovered a large lake under the Manson Icefield in the Canadian Arctic. Early in 2021 the ice surface over the center of the lake sank by around 140 m implying a total subglacial water outflow of around 4 km^3, the largest reported outside of Iceland and Antarctica. Most of this water drained from the subglacial lake within 30 days melting some of the ice along the outflow path. For the first time we map the position and size of the subglacial output channel between the downstream end of the lake and the ocean using post-outflow surface depression as the ice sank downward to close the channel after the water outflow. These results help in understanding the ways in which the presence, movement, and volume of water beneath glaciers influence ice movement and climate related glacial ice loss.

1. Introduction

Subglacial lakes play a key role in freshwater storage and ice dynamics. The ways in which they fill and empty is important in understanding subglacial hydrology and its role in glacial ice dynamics and climate related ice loss. Subglacial lakes exist under ice caps (Björnsson, 2003; Liang et al., 2022; Willis et al., 2015) and the Greenland and Antarctic ice sheets (Bell et al., 2007; Fricker et al., 2007; Livingstone et al., 2022; Siegert, 2000; Smith et al., 2009). In a recent review of subglacial lakes, Livingstone et al. (2022) found that around 20% of all known subglacial lakes were 'active', with ice surface height changes associated with cyclic filling and emptying. For the active subglacial lakes, they showed that the slow fill and rapid drainage pattern tended to produce the largest discharge rates and volumes.

One of the best studied examples of a slow fill, rapid outflow subglacial lake is in Iceland where geothermal energy creates a subglacial lake in the Grímsvötn caldera under the Vatnajökull ice cap and the slow build-up of water from melting ice eventually leads to periodic outburst floods, or jökulhlaups (Björnsson, 2003; Guðmundsson et al., 2004). Other examples of episodic filling and outflow from subglacial lakes exist in Antarctica (Fricker et al., 2007; Smith et al., 2009) and Greenland (Bowling et al., 2019; Fan et al., 2023; Gray et al., 2024). Outburst floods from subglacial lakes have rarely been observed in the Canadian Arctic, although in 1978 an outburst flood drained Hazard Lake through a subglacial tunnel beneath Steele Glacier, Yukon Territory (Clarke, 1982), and repeated outburst floods drained into Lake Tuborg on Ellesmere Island from a glacier-dammed ice marginal lake (Lewis et al., 2009; Smith et al., 2004).

19448007, 2024, 19, Downloaded from https://agupubs.onlinelibrary.wiley.com/doi/10.1029/2024GL110456, Wiley Online Library on [07/10/2024]. See the Terms and Conditions (https://onlinelibrary.wiley.com/terms-and-conditions) on Wiley Online Library for rules of use; OA articles are governed by the applicable Creative Commons License

Here we describe a large active subglacial lake under Manson Icefield on southern Ellesmere Island, the first of its kind documented in Canada and one of the largest documented anywhere outside of Antarctica. In the current work, and in a recent study of a large subglacial lake in NE Greenland (Gray et al., 2024), the slow-fill, rapid drainage pattern is observed with outflow volumes of order 1 km^3, outflow and refill times of order days and years respectively, and average outflow rates of order 10^3 $m^3 s^{-1}$. The data provides insights into both the timing and magnitude of the outburst flood, as well as the subglacial hydrologic routing of the drainage. While we lack the data for quantitative outflow modeling, the observations are discussed in the context of the theories of subglacial water movement which originally suggested channels (Nye, 1976; Röthlisberger, 1972), or 'sheet flow' (Weertman, 1972). More recent models allow both channels and linked cavities or equivalent efficient and inefficient drainage systems (De Fleurian et al., 2018; Schoof, 2010; Werder et al., 2013).

2. Data and Methods

We use ICESat-2 ATL06 land ice height measurements (Smith and others, 2023) and time referenced ArcticDEM strips from the University of Minnesota Polar Geospatial Center (PGC) (Noh and Howat, 2014, 2015; Porter et al., 2022) to provide geolocated surface heights above the WGS84 ellipsoid. Details of both the ICESat-2 and DEM data manipulation are contained in the supporting material.

Subglacial lake outflow has the potential to influence ice movement both above and downstream from the subglacial lake so we used ITS_LIVE data (Gardner et al., 2018, 2023; Lei et al., 2022) to monitor surface ice displacements before, during and after the large water outflow (Joughin, 2002). Details of the data manipulation are included in the supporting material.

3. Results

Figure 1 shows the location of the subglacial lake under Manson Icefield at the southern end of Ellesmere Island. The lake outline in Figure 1a was estimated based on the location where the height difference between the pre- and post-outflow DEMs in Figure 1d approached zero. This was checked against the Sentinel-2 image from 5 August 2021 where the north and south edges could be identified.

All the DEMs show that the lake area lies in a basin such that the surface height at the center of the lake is below the heights at both the east and west ends. Eight glaciers feed the basin and a fraction of the western arm of Mittie Glacier is also diverted into the lake basin at the south-east end of the yellow lake boundary. The ITS_LIVE yearly displacement data (Figure S1 in Supporting Information S1) and surface slope imply that there is no glacial ice outflow from the basin.

3.1. Temporal Height and Volume Change

Figure 1 illustrates the ice surface elevation change based on a sequence of DEMs. The earliest profile, in red in Figure 1e, is from spring 2012 and shows an ice surface elevation of around 200 m in the middle of the lake. The surface elevation then increases and the highest profile is from 16 September 2020. The two lowest profiles are from 8 March and 18 May 2021 showing that there must have been a major outflow between 16 September 2020 and 8 March 2021. The 2022 profile shows that the subglacial lake is beginning to fill after the outflow in late 2020 or early 2021.

We can refine the dates of the major outflow using ICESat-2data. Figure 2a includes two areas that were covered repeatedly by ICESat-2 where the ice was supported by water even after the major outflow. The height difference between these passes and the height of the pre-outflow DEM from 7 April 2020 at the positions of the ICESat-2 data is used to estimate the temporal surface height change. The plots in Figure 2b show a small height decrease from 3 February 2020–31 January 2021, but the major decrease in elevation occurred after this. The irregular topography revealed by overlapping profiles at 0.6–1.2 km in Figure 2b indicates that between 31 October 2021 and January 2023 the ice is now not floating at that location.

Some of the descending tracks covering area 2 are plotted in Figure 2c. These plots confirm that the level of the glacier surface had not dropped significantly on 6 January 2021 but had by 7 April 2021. All the available ICESat-2 and DEM height change results with respect to the 7 April 2020 DEM are combined in Figure 2d. The ICESat-2 points are averages of line segments within the two areas and the values for the DEMs are averaged over the two areas. Figure 2d shows that the outflow may have just started in January 2021. By 3 February 2021 the level had

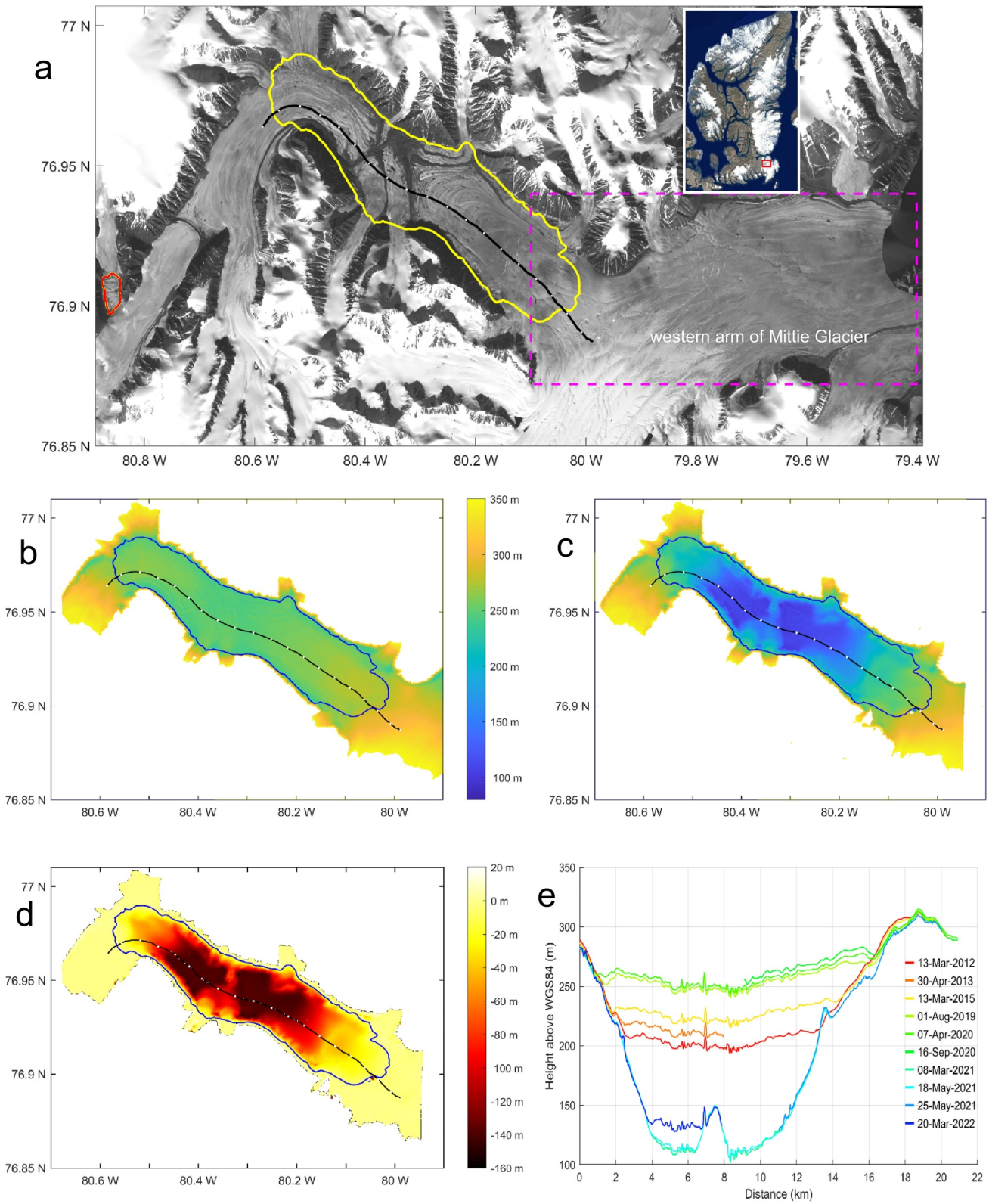

Figure 1.

19448007, 2024, 19, Downloaded from https://agupubs.onlinelibrary.wiley.com/doi/10.1029/2024GL110456, Wiley Online Library on [07/10/2024]. See the Terms and Conditions (https://onlinelibrary.wiley.com/terms-and-conditions) on Wiley Online Library for rules of use; OA articles are governed by the applicable Creative Commons License

19448007, 2024, 19, Downloaded from https://agupubs.onlinelibrary.wiley.com/doi/10.1029/2024GL110456, Wiley Online Library on [07/10/2024]. See the Terms and Conditions (https://onlinelibrary.wiley.com/terms-and-conditions) on Wiley Online Library for rules of use; OA articles are governed by the applicable Creative Commons License

dropped by around 10 m from 5 January, and then dropped a further 130 m by 6 March 2021, that is, in a period of 30 days.

The surface area of the top of the subglacial lake, indicated by the yellow outline in Figure 1a, was estimated based on the difference of DEMs from spring 2020 (Figure 1b) and spring 2021 (Figure 1c). However, Figure 2d shows that the ice surface above the lake continued to rise during the summer and fall of 2020. This may have increased the maximum lake area beyond the 52.2 ± 2 km^2 value quoted above. The additional water would have made little difference to the width of the lake because of the steep topography at the sides but may have increased its area at the eastern end depending on the bed slope. While we cannot estimate the area increase, we can use the original area to estimate the additional volume of water which entered the lake in the summer and fall of 2020. The pre-outflow DEM minus the post-outflow DEM implies a volume change of 3.92 ± 0.2 km^3. The 5 m height increase between spring 2020 and the end of 2020 indicates an additional water contribution of 0.26 km^3. This suggests a total volume output of 4.18 ± 0.2 km^3 at the time of lake drainage.

After the large outflow early in 2021 a large crevasse was created running across the glacier ice cover, which is marked with a white arrow in Figure 2a. As the lake level dropped, the ice must have settled onto the bed such that the ice surface was under sufficient longitudinal stress to create the crevasse. The feature is also visible as the local peak in the surface height change plot (Figure 1e) from 25 May 2021 at 13.5 km.

We searched historical imagery to find the last time there was clear evidence of a crevasse at this location. With ERS-1 imagery we can see what appears to be a post-outflow crevasse on 20 September 1993 which is not visible on a Landsat image from 9 July 1993, suggesting that a large outflow happened between these dates. Height change using ASTER DEMs (Figure 2d) shows that there must have also been an outflow between 10 July 2006 and 30 July 2009. Examination of surface features, including crevassing and supraglacial and ice-marginal lakes in Landsat imagery, suggests that the most likely period for the outflow was between 29 August 2007 and 17 June 2008. These dates for the last three outflow events imply that recently there has been approximately 14 years between major outflows.

3.2. Subglacial Water Outflow Channel

The large water outflow in 30 days suggests that there would be a subglacial channel or channels draining the lake. By differencing DEMs we found a significant surface depression that appeared following the drainage event, implying subglacial ice melt and subsequent post-outflow downward movement of ice above the region of ice melt. Figure 3a illustrates the height difference between a pre-outflow DEM and a post-outflow DEM of the area downstream from the subglacial lake. The pre-outflow DEM is a combination of ArcticDEMs from 29 August 2020 and 16 September 2020 while the post-outflow DEM is a combination of ArcticDEMs from 7 May 2021 and 28 August 2021. There was height change due to summer 2021 surface melt and biases of 0.5 and 2.5 m have been used in the two parts of the post-outflow DEM to isolate the height change associated with the subglacial melt related surface depression and exclude the height change associated with surface melt.

Figure 3a shows a surface depression which begins as a broad feature just downstream from the lake edge. Then at around 80°W the feature appears to form a single pathway with surface depression up to ∼3.5 m, although there is a short 1 km section with negligible surface depression. Further downstream, the surface depression is 600–800 m wide and up to ∼3 m deep. The ICESat-2 profiles show that this surface depression is related to the timing of the outflow; all the profiles along P1 after 30 March 2021 in Figure 3b show the distinct and repeatable surface depression.

Each of the five post-outflow plots in Figures 3b, 3c and 3d illustrate the height change for the three positions on the same date. On 30 March 2021, the surface depression appeared to be fully developed at position P1, partially

Figure 1. (a): The shape of the subglacial lake when nearly full is shown as the yellow outline on part of a Sentinel 2 image from 5 August 2021. The location of the lake in Manson Icefield at the southeastern end of Ellesmere Island is shown in the inset image by the small red box. The red outline at west side of (a) at 76.9 N illustrates the extent of another small active subglacial lake discussed in the text. The dashed magenta line shows the location of Figure 3a (b) Pre-outflow surface height from a DEM from 7 April 2020. (c) Post-outflow height from a composite of DEMs from 8 March 2021 and 25 May 2021 shown using the same color bar as in (b). (d): Surface height difference between the pre- and post-outflow heights. (e) Surface heights interpolated from the available DEMs along the black profile in (a) to (d). The profiles run from the NW to SE and the white dots are separated by 1 km and allow for comparison with the *x* axis in (e). The lowest profile from 8 March 2021 is the first height profile after the outburst flood.

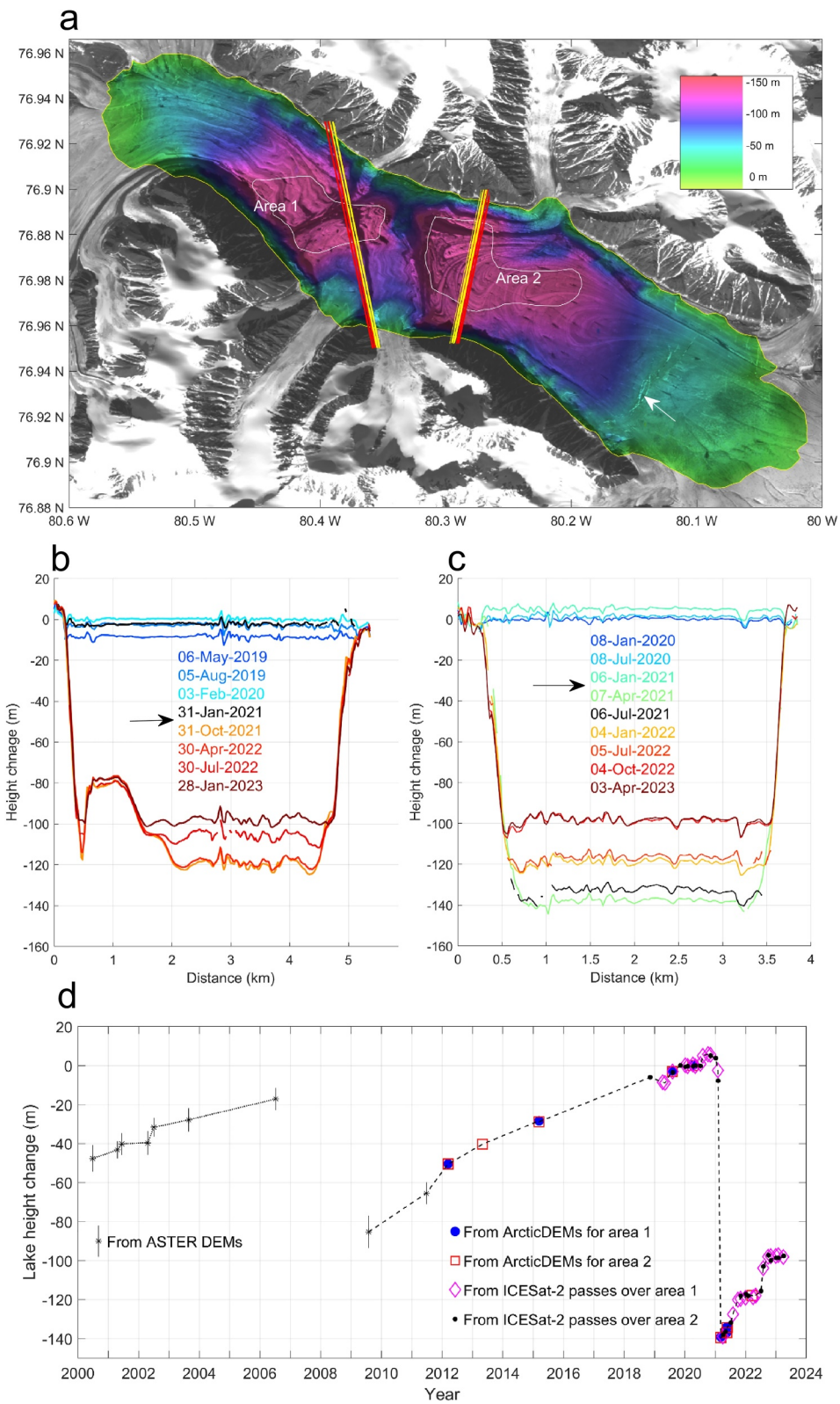

Figure 2.

19448007, 2024, 19, Downloaded from https://agupubs.onlinelibrary.wiley.com/doi/10.1029/2024GL110456, Wiley Online Library on [07/10/2024]. See the Terms and Conditions (https://onlinelibrary.wiley.com/terms-and-conditions) on Wiley Online Library for rules of use; OA articles are governed by the applicable Creative Commons License

19448007, 2024, 19, Downloaded from https://agupubs.onlinelibrary.wiley.com/doi/10.1029/2024GL110456, Wiley Online Library on [07/10/2024]. See the Terms and Conditions (https://onlinelibrary.wiley.com/terms-and-conditions) on Wiley Online Library for rules of use; OA articles are governed by the applicable Creative Commons License

developed at P2, but only beginning to develop at P3. The next date with good ICESat-2 data was the 27 December 2021, 3 orbit cycles later when the surface depression was slightly deeper at P2 and much deeper at P3. There appears to be little change in depression shape the following spring on 28 March 2022. These observations are discussed in the following section. Although the profiles at each date have been offset downward by 2 m in Figure 3 to avoid overlap, the comparison of height changes between P1, P2 and P3 also illustrate the increased surface melt as the surface elevation decreases toward the ocean. The track of the surface depression does not follow a surface melt water path (see supplementary Figure S4d in Supporting Information S1).

The delta shaped area of enhanced surface height loss at the end of the channel in Figure 3a is not a consequence of the outburst flood. By comparing pre-outflow DEMs from August 2020 and September 2012 we see the same pattern of height loss, but with a larger magnitude due to the longer time separation between the DEMs (supporting material Figure S4b in Supporting Information S1). This figure also shows enhanced surface depression at the ice margin at the position of the end of the channel, suggesting that previous outburst floods may have followed, or at least ended at, a similar location. Also, the data from a descending ICESat-2 pass shows the progression of height loss across this region both before and after the outburst flood. These data show that the surface depression and the subglacial channel must extend through this region to the glacier terminus. The surface depression in this region appears first in the 31 December 2021 ICESat-2 track and then in the 31 March 2022, 29 September 2022 and 30 March 2023 tracks (Figure S4d in Supporting Information S1). Interestingly, the depth of the melt induced surface depression appears to be larger in the later three passes than in the 31 December 2021 pass.

3.3. Ice Movement Before, During and After the Outburst Flood

To assess whether the outburst flood influenced the downstream ice motion ITS_LIVE ice motion products (Gardner et al., 2023) have been examined. The yearly composites from 2020, 2021 and 2022 show that the ice motion above the position of the subglacial channel was slow (<∼10 m/year) and becomes essentially stagnant close to the glacier terminus for all 3 years. Change in ice motion can also be monitored using imagery separated by much shorter time periods, for example, the 16 days used for the 'Hovmöller' plot (supplementary plot S2 in Supporting Information S1), which does not show any significant difference in surface motion above the outflow path in the February to March time frame for the 3 years.

Vertical ice motion over the subglacial lake can be detected using ITS_LIVE speckle tracking products using the methodology outlined in the supporting information. Supplementary Figure S3 in Supporting Information S1 summarizes these results and shows that the rate of ice surface decrease above the lake, and therefore outflow, is still increasing early to mid-February but has decreased significantly by the end of February 2021.

3.4. Additional Evidence for Episodic Subglacial Water Movement in the Area

In Figure 1a there is a small subglacial lake at the western end of the image which has been outlined in red. While much smaller than the main lake, ICESat-2 coverage shows that the ice surface above this lake dropped from ∼440 to ∼330 m sometime between 8 June 2019 and 8 November 2019. After the sudden drop in surface elevation the height increased from ∼334 m on 7 March 2020 to ∼383 m by 7 August 2020. This was followed by more modest height increases in the summers of 2021 and 2022. Another area with an anomalous height increase of ∼13 m between 5 May 2021 and 8 August 2021 is marked by a white arrow in Figure 3a.

4. Discussion and Conclusions

The situation on Manson Icefield where glacial ice only flows into the subglacial lake basin is unusual but not unique. Further north on Ellesmere Island the active subglacial lake identified as the source of the outburst floods

Figure 2. (a): The surface height difference between the DEMs in Figure 1b (7 April 2020) and 1c (combination of 8 March 2021 and 25 May 2021) is illustrated as a color overlay superimposed on a post-outflow Sentinel 2 image from 5 August 2021. The red and yellow lines crossing area 1 are ICESat-2 tracks for left and right beam 1 from an ascending track, and the red and yellow lines through area 2 are tracks for beam 3 from a descending track. Plots of the height difference in meters between ICESat-2 and the 7 April 2020 DEM are shown for (b) Area 1 and (c) Area 2. The arrows show the time of the outburst flood. (d) The height change history with respect to the surface height defined by the 7 April 2020 DEM.

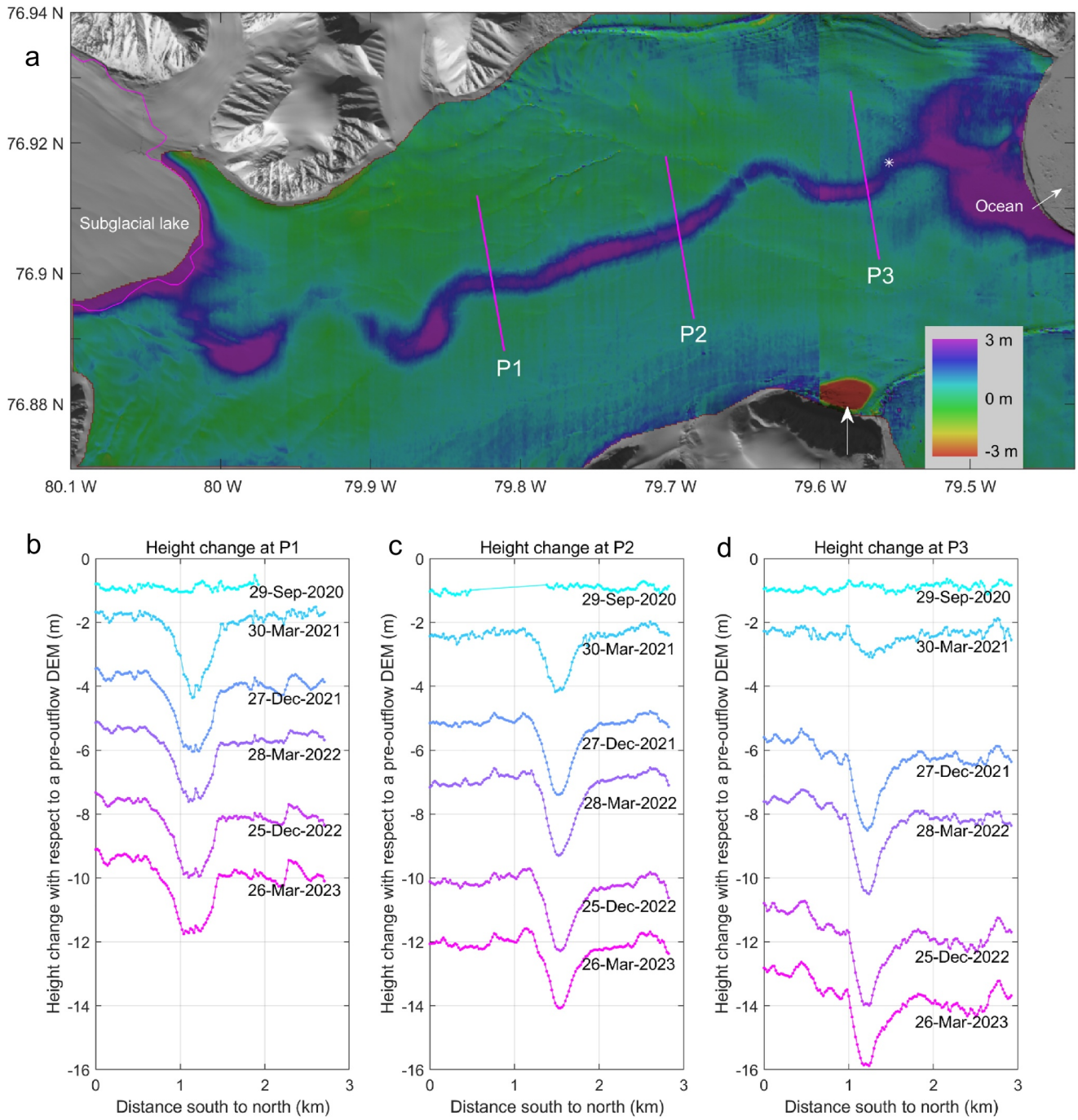

Figure 3. (a): Height difference between a pre-outflow summer 2020 DEM and a post-outflow spring/summer 2021 DEM. Background image is from Sentinel 2, 5 August 2021. The small white asterix just downstream of the P3 profile is the position of the ice thickness estimate discussed in the text. (b), (c) and (d) illustrate the height difference between the pre-outflow DEM and the 6 ICESat-2 passes from a sequence of days from 20 September 2020–26 March 2023 at the position of the three profiles P1, P2 and P3. The three plots for each date correspond to the left beam from the three reference tracks. For clarity each of the plots in (b), (c) and (d) has been offset downward by an additional 2 m relative to the previous plot. The outburst flood occurred at a time between the top two profiles.

entering Tuborg Lake (Lewis et al., 2009; Smith et al., 2004) is also in a basin in which ice flow apparently converges.

On Manson the water level in the subglacial lake increased until sometime in January 2021 when leakage began at the eastern end of the subglacial lake. While slow at first, this water outflow begins to erode a channel and leads to

19448007, 2024, 19, Downloaded from https://agupubs.onlinelibrary.wiley.com/doi/10.1029/2024GL110456, Wiley Online Library on [07/10/2024]. See the Terms and Conditions (https://onlinelibrary.wiley.com/terms-and-conditions) on Wiley Online Library for rules of use; OA articles are governed by the applicable Creative Commons License

19448007, 2024, 19, Downloaded from https://agupubs.onlinelibrary.wiley.com/doi/10.1029/2024GL110456, Wiley Online Library on [07/10/2024]. See the Terms and Conditions (https://onlinelibrary.wiley.com/terms-and-conditions) on Wiley Online Library for rules of use; OA articles are governed by the applicable Creative Commons License

some ice melting which then leads to increasing outflow, more melting, and the fast-outflow pattern characteristic of Icelandic jökulhlaups (Livingstone et al., 2022; Nye, 1976; Tweed & Russell, 1999). While our data on the temporal discharge are limited (Figure S3d in Supporting Information S1), they do not appear to duplicate the initial discharge attributed to sheet flood drainage of the 1996 jökulhlaup from subglacial Lake Grimsvötn in Iceland (Flowers et al., 2004). The fast water outflow at the eastern end of the lake began around the start of February 2021, peaked in the middle of February and ended early in March. While Sentinel-1 radar imagery did show signs of upwelling at the glacier terminus during the February-March 2021 time frame, it was not possible to identify the timing of the peak outflow to the ocean.

It is perhaps surprising that the large outburst flood does not appear to influence the surface ice speed during or after the flood, especially when there is a wealth of information showing that subglacial water does influence ice movement (e.g., Armstrong et al., 2016; Bartholomaus et al., 2008; Iken & Bindschadler, 1986; Schoof, 2010). Indeed, Yang et al. (2022) documented an example in Alaska where an outburst flood did lead to a significant increase in ice speed. While a one-to-one comparison of the basal channel size with the surface depression may not be 100% accurate, we can use the surface subsidence data to postulate that the outflow did create a single, wide (600–800 m) and shallow (<3.5 m) subglacial pathway. The limited extent of the subglacial channel in relation to the width of the glacier coupled with the low pre-outflow ice speed downstream of the subglacial lake, and essentially stagnant ice close to the terminus of the western arm of Mittie Glacier, suggests that the outburst flood could not influence the basal drag for enough of the ice to affect the overall ice speed. This supports our contention that the outflow is efficient, and that the transit time for water passing through the channel would more likely be of order days, rather than weeks.

Supplementary Figure S4d in Supporting Information S1 show that height loss continues inside the delta shaped enhanced surface height loss region close to the ice edge during the winter of 2019–2020, but not outside this area. This suggests that there is sea water incursion into the extended purple area in Figure 3a leading to the enhanced height loss. As the glacial ice there may be close to floatation, these observations point the way to an explanation of the different rates of channel closure revealed by the plots (Figures 3b–3d) at P1, P2 and P3 from 30 March 2021.

When the water outflow came to a stop, and this was well before 30 March 2021, the presence of ocean water at the end of the open tunnel guarantees that there would be water present in the tunnel and pressure acting against the overburden weight of the ice trying to close the tunnel. On 4 May 2012, the NASA IceBridge program flew a transect across the glacier close to the terminus providing one position where we can estimate ice thickness and bed height. This is marked by a white asterisk in Figure 3a and is around 1 km downstream from the intersection of the P3 profile and the subglacial tunnel position, but not into the region of enhanced height loss. Accounting for height loss since 2012 due to surface melt, the ice thickness just post outflow at this location is ∼280 m, and the surface ice height is ∼100 m above the WGS84 ellipsoid and ∼91 m above mean sea level. As sea level will then be ∼189 m above this position, the water pressure in the tunnel will be significant, approximately 75% of the overburden ice pressure. Assuming an unimpeded water connection to the ocean, as one goes from P3 to P2 to P1 the ice surface height increases and the effective pressure, the difference between the overburden pressure and the water pressure, must increase. This could explain the different closure rates for the three positions. The progression of surface depression in the region of enhanced melt at the glacier terminus (Figure S4d in Supporting Information S1) supports this interpretation. Here we see that the surface depression appears to increase after 31 December 2021. The 29 September 2022 and 30 March 2023 plots are similar and show increased surface depression in relation to the December 2021 plot. These observations imply an even slower rate of channel closure than at P3. This is consistent with the expected decrease in post-outflow effective pressure in the channel close to the glacier terminus, particularly through the expected increase in water pressure. It is also possible that prior to the closure of the tunnel at the glacier terminus, tidal forces could create some water movement in the tunnel, with associated ice loss.

Historical image data has allowed us to show that in the last few decades the period of the fill—outflow cycle is around 14 years. While the size of this subglacial lake and the periodic outflow may be exceptional, there is little doubt that other active subglacial lakes are present in the Canadian Arctic. Even in the part of Manson Icefield illustrated in Figure 1a there is one other confirmed active subglacial lake and another area with unusual height change which suggests that this too may be an active subglacial lake.

19448007, 2024, 19, Downloaded from https://agupubs.onlinelibrary.wiley.com/doi/10.1029/2024GL110456, Wiley Online Library on [07/10/2024]. See the Terms and Conditions (https://onlinelibrary.wiley.com/terms-and-conditions) on Wiley Online Library for rules of use; OA articles are governed by the applicable Creative Commons License

This study is unique in providing details of the episodic subglacial outflow from a large active subglacial lake in the Canadian Arctic, and in showing the size and shape of much of the subglacial channel through which the water flows to the ocean. After the outburst flood, different channel closure rates appear to depend on the effective pressure, the difference between the ice overburden and water pressure in the tunnel due to the channel height below sea level.

Data Availability Statement

ATL06 land ice height measurements (Smith and others, 2023) from ICESat-2 are available from NSIDC (https://nsidc.org/data/atl06/versions/6). The time referenced DEMs were downloaded from the Polar Geospatial Center (PGC) of the University of Minnesota (https://data.pgc.umn.edu/elev/dem/setsm/ArcticDEM/strips/s2s041/). The ASTER DEMs were generated using MicMac ASTER (Girod and others, 2017) using ASTER Level 1A reconstructed instrument data downloaded from NASA Earth Data (www.earthdata.nasa.gov/). The Landsat imagery was acquired from the Earth Explorer site of the US Geological Service (https://earthexplorer.usgs.gov/). The ITS_LIVE data are provided by the NASA MEaSUREs ITS_LIVE project (https://its-live.jpl.nasa.gov/, Gardner et al., 2023). Sentinel-2 imagery is available from https://www.esa.int/Applications/Observing_the_Earth/Copernicus/Sentinel-2/Sentinel-2_downloads. The profile of ice thickness data across Mittie Glacier was downloaded from the NASA IceBridge Data Portal https://nsidc.org/icebridge/portal.

Acknowledgments

Stephen Livingstone, Sian Thorpe and William Armstrong provided constructive and helpful comments which improved our paper. Their help, and that of the editor, Mathieu Morlighem, is gratefully appreciated. Dr C. Dow was supported by the Canada Research Chairs Program (950–231237) and the NSERC of Canada Discovery Grant program (RGPIN-03761-2017). Support for L. Copland, W. Van Wychen and K. Alley was provided by NSERC Discovery Grants, RGPIN-2023-05639, RGPIN-2021-02443 and RGPIN-2021-02910, respectively. B. Lauzon was supported by the Natural Sciences and Engineering Research Council of Canada and Polar Knowledge Canada.

References

Armstrong, W. H., Anderson, R. S., Allen, J., & Rajaram, H. (2016). Modeling the WorldView-derived seasonal velocity evolution of Kennicott glacier, Alaska. *Journal of Glaciology*, *62*(234), 763–777. https://doi.org/10.1017/jog.2016.66

Bartholomaus, T., Anderson, R., & Anderson, S. (2008). Response of glacier basal motion to transient water storage. *Nature Geoscience*, *1*, 33–37. https://doi.org/10.1038/ngeo.2007.52

Bell, R. E., Studinger, M., Shuman, C. A., Fahnestock, M., & Joughin, I. (2007). Large subglacial lakes in East Antarctica at the onset of fast-flowing ice streams. *Nature*, *445*(7130), 904–907. https://doi.org/10.1038/nature05554

Björnsson, H. (2003). Subglacial lakes and jökulhlaups in Iceland. *Global and Planetary Change*, *35*(3–4), 255–271. https://doi.org/10.1016/S0921-8181(02)00130-3

Bowling, J. S., Livingstone, S. J., Sole, A. J., & Chu, W. (2019). Distribution and dynamics of Greenland subglacial lakes. *Nature Communications*, *475*(10), 1–12. https://doi.org/10.1038/s41467-019-10821-w

Clarke, G. K. C. (1982). Glacier outburst floods from "Hazard Lake". *Yukon Territory, and the Problem of Flood Magnitude Prediction. Journal of Glaciology*, *28*(98), 3–21. https://doi.org/10.3189/S0022143000011746

De Fleurian, B., Werder, M. A., Beyer, S., Brinkerhoff, D. J., Delaney, I. A. N., Dow, C. F., et al. (2018). SHMIP the subglacial hydrology model intercomparison Project. *Journal of Glaciology*, *64*(248), 897–916. https://doi.org/10.1017/jog.2018.78

Fan, Y., Ke, C. Q., Shen, X., Xiao, Y., Livingstone, S. J., & Sole, A. J. (2023). Subglacial lake activity beneath the ablation zone of the Greenland Ice Sheet. *The Cryosphere*, *17*(4), 1755–1786. https://doi.org/10.5194/tc-17-1775-2023

Flowers, G. E., Björnsson, H., Pálsson, F., & Clarke, G. K. C. (2004). A coupled sheet-conduit mechanism for jökulhlaup propagation. *Geophysical Research Letters*, *31*(5), L05401. https://doi.org/10.1029/2003GL019088

Fricker, H. A., Scambos, T., Bindschadler, R., & Padman, L. (2007). An active subglacial water system in west 509 Antarctica mapped from space. *Science*, *315*(5818), 1544–1548. https://doi.org/10.1126/science.1136897510

Gardner, A. S., Fahnestock, M. A., & Scambos, T. A. (2023). ITS_LIVE regional glacier and ice sheet surface velocities: Version 1. *Data archived at National Snow and Ice Data Center*. https://doi.org/10.5067/6II6VW8LLWJ7

Gardner, A. S., Moholdt, G., Scambos, T., Fahnestock, M., Ligtenberg, S., van den Broeke, M., & Nilsson, J. (2018). Increased West Antarctic and unchanged East Antarctic ice discharge over the last 7 years. *The Cryosphere*, *12*(2), 521–547. https://doi.org/10.5194/tc-12-521-2018

Girod, L., Nuth, C., Kääb, A., McNabb, R., & Galland, O. (2017). Mmaster: Improved ASTER DEMs for elevation change monitoring. *Remote Sensing*, *9*(7), 704. https://doi.org/10.3390/rs9070704

Gray, L., Burgess, D., Copland, L., Dow, C., Fettweiss, X., Fisher, D., et al. (2024). Repeated subglacial jökulhlaups in northeastern Greenland revealed by CryoSat. *Journal of Glaciology*, 1–24. Published online 2024. https://doi.org/10.1017/jog.2024.32

Guðmundsson, M. T., Sigmundsson, F., Bjornsson, H., & Hognadottir, T. (2004). The 1996 eruption at Gjalp, Vatnajokull ice cap, Iceland: Efficiency of heat transfer, ice deformation and subglacial water pressure. *Bulletin of Volcanology*, *66*(1), 46–65. https://doi.org/10.1007/s00445-003-0295-9

Iken, A., & Bindschadler, R. A. (1986). Combined measurements of subglacial water pressure and surface velocity of findelengletscher, Switzerland: Conclusions about drainage system and sliding mechanism. *Journal of Glaciology*, *32*(110), 101–119. https://doi.org/10.3189/S0022143000006936

Joughin, I. (2002). Ice-sheet velocity mapping: A combined interferometric and speckle-tracking approach. *Annals of Glaciology*, *34*, 195–201. https://doi.org/10.3189/172756402781817978

Lei, Y., Gardner, A. S., & Agram, P. (2022). Processing methodogy for the ITS_LIVE Sentinel-1 velocity products. *Earth System Science Data*, *14*(11), 5111–5137. https://doi.org/10.5194/essd-14-5111-2022

Lewis, T., Francus, P., & Bradley, R. S. (2009). Recent occurrence of large jökulhlaups at Lake Tuborg, Ellesmere Island, Nunavut. *Journal of Paleolimnology*, *41*(3), 491–506. https://doi.org/10.1007/s10933-008-9240-4

Liang, Q., Xiao, W., Howat, I., Cheng, X., Hui, F., Chen, Z., et al. (2022). Filling and drainage of a subglacial lake beneath the Flade Isblink ice cap, northeast Greenland. *The Cryosphere*, *16*(7), 2671–2681. https://doi.org/10.5194/tc-16-2671-2022

Livingstone, S. J., Li, Y., Rutishauser, A., Sanderson, R. J., Winter, K., Mikuchi, J. A., et al. (2022). Subglacial lakes and their changing role in a warming climate. *Nature Reviews Earth and Environment*, *3*(2), 106–124. https://doi.org/10.1038/s43017-021-00246-9

Noh, M. J., & Howat, I. M. (2014). Automated coregistration of repeat digital elevation models for surface elevation change measurement using geometric constraints. *IEEE Transactions on Geoscience and Remote Sensing*, *52*(4), 2247–2260. https://doi.org/10.1109/TGRS.2013.2258928

Noh, M. J., & Howat, I. M. (2015). Automated stereo-photogrammetric DEM generation at high latitudes: Surface Extraction from TIN-Based Search Minimization (SETSM) validation and demonstration over glaciated regions. *GIScience and Remote Sensing*, *52*(2), 198–217. https://doi.org/10.1080/15481603.2015.1008621

Nye, J. F. (1976). Water flow in glaciers: Jökulhlaups, tunnels and veins. *Journal of Glaciology*, *17*(76), 181–207. https://doi.org/10.3189/S002214300001354X

Porter, C., Howat, I., Noh, M. J., Husby, E., Khuvis, S., Danish, E., et al. (2022). ArcticDEM – strips, version 4.1. https://doi.org/10.7910/DVN/C98DVS. Harvard Dataverse, V1.

Röthlisberger, H. (1972). Water pressure in intra- and subglacial channels. *Journal of Glaciology*, *11*(62), 177–203. https://doi.org/10.3189/S0022143000022188

Schoof, C. (2010). Ice-sheet acceleration driven by melt supply variability. *Nature*, *468*(7325), 803–806. https://doi.org/10.1038/nature09618

Siegert, M. J. (2000). Antarctic subglacial lakes. *Earth-Science Reviews*, *50*(1), 29–50. https://doi.org/10.1016/S0012-8252(99)00068-9

Smith, B., Adusumilli, S., Csathó, B. M., Felikson, D., Fricker, H. A., Gardner, A., et al. (2023). *ATLAS/ICESat-2 L3A land ice height, version 6*. NASA National Snow and Ice Data Center Distributed Active Archive Center. https://doi.org/10.5067/ATLAS/ATL06.006

Smith, B., Fricker, H., Joughin, I., & Tulaczyk, S. (2009). An inventory of active subglacial lakes in Antarctica 589 detected by ICESat (2003–2008). *Journal of Glaciology*, *55*(192), 573–595. https://doi.org/10.3189/002214309789470879591

Smith, S. V., Bradley, R. S., & Abbott, M. B. (2004). A 300 year record of environmental change from Lake Tuborg, Ellesmere Island, Nunavut, Canada. *Journal of Paleolimnology*, *32*(2), 137–148. https://doi.org/10.1023/B:JOPL.0000029431.23883.1c

Tweed, F. S., & Russell, A. J. (1999). Controls on the formation and sudden drainage of glacier-impounded lakes: Implications for jo¨kulhlaup characteristics. *Progress in Physical Geography*, *23*(1), 79–110. https://doi.org/10.1177/030913339902300104

Weertman, J. (1972). General theory of water flow at the base of a glacier or ice sheet. *Reviews of Geophysics*, *10*(1), 287–333. https://doi.org/10.1029/RG010i001p00287

Werder, M. A., Hewitt, I. J., Schoof, C. G., & Flowers, G. E., (2013). Modeling channelized and distributed subglacial drainage in two dimensions. *J. Geophys. Res.Earth Surface*, *118*(1), 2140–2158. https://doi.org/10.1002/jgrf.20146

Willis, M. J., Herried, B. G., Bevis, M. G., & Bell, R. E. (2015). Recharge of a subglacial lake by surface meltwater in northeast Greenland. *Nature*, *518*(7538), 223–227. https://doi.org/10.1038/nature14116

Yang, R., Hock, R., Kang, S., Guo, W., Shangguan, D., Jiang, Z., & Zhang, Q. (2022). Glacier surface speed variations on the Kenai Peninsula, Alaska, 2014–2019. *Journal of Geophysical Research: Earth Surface*, *127*(3), e2022JF006599. https://doi.org/10.1029/2022jf006599

19448007, 2024, 19, Downloaded from https://agupubs.onlinelibrary.wiley.com/doi/10.1029/2024GL110456, Wiley Online Library on [07/10/2024]. See the Terms and Conditions (https://onlinelibrary.wiley.com/terms-and-conditions) on Wiley Online Library for rules of use; OA articles are governed by the applicable Creative Commons License